Int. J. Electrochem. Sci., 14 **(2019)** 3443 – 3454, doi: 10.20964/2019.04.50

International Journal of
ELECTROCHEMICAL
SCIENCE
www.electrochemsci.org

Synthesis, Crystal Structure and Corrosion Inhibition Effect of S-benzyl-O,O'-bis(*p*-tert-butyl phenyl)dithiophosphate for Q235 Steel in 1.0 M HCl

Chengduan Wang[1], *Wan Gou*[1], *Changlu Liu*[1], *Dong Fu*[1], *Lvshan Zhou*[1], *Chuan Lai*[1,2*], *Bin Xie*[2,*], *Shasha Zhu*[2]

[1] Eastern Sichuan Sub-center of National Engineering Research Center for Municipal Wastewater Treatment and Reuse, Sichuan University of Arts and Science, Dazhou 635000, China
[2] School of Materials Science and Engineering, Sichuan University of Science and Engineering, Zigong 643000, China
[*]E-mail: laichuanemail@163.com; xiebinsuse@163.com

Received: 13 August 2018 / *Accepted:* 18 October 2018 / *Published:* 10 March 2019

The new corrosion inhibitor of S-benzyl-O,O'-bis(*p*-tert-butyl phenyl)dithiophosphate (SOBP) was synthesized and characterized by elemental analysis, FT-IR, ^{1}H NMR, ^{13}C NMR, ^{31}P NMR and single crystal X-ray diffraction. Meanwhile, the corrosion inhibition and mechanism of SOBP for Q235 steel in 1.0 M HCl were studied by weight loss and potentiodynamic polarization measurement, also the crystal structure of corrosion inhibitor was presented. The potentiodynamic polarization measurement result indicates that SOBP is a mixed-type inhibitor. The two methods all reveal that the inhibition efficiency increases with the concentration of SOBP, which is an effective corrosion inhibitor. The adsorption of SOBP on Q235 steel surface in 1.0 M HCl belongs both physisorption and chemisorption.

Keywords: Synthesis; Structure; Corrosion; Steel; Hydrochloric acid.

1. INTRODUCTION

Metal materials are most important engineering materials, but the corrosion phenomena are widely presented in various fields for using [1-3]. Among many metal materials, the different types of steel have been outstanding in application due to its unique advantages. However, while it is widely used, the corrosion also brings many limitations. This is not only because corrosion lead to damage, environmental pollution and resource waste, but more importantly, it can cause major safety hazards.

Therefore, the metal materials corrosion is not only an economic problem, but also a social problem [4-6].

At present, there are many of the techniques to prevent or slow down the corrosion of materials, in these methods, using inhibitors has become an important method to slow down the corrosion of metal pickling due to its advantages of simple, convenient and economical [7-9]. Inhibitors can effectively inhibit corrosion for adding it in corrosive medium, and which can be divided into organic and inorganic corrosion inhibitors. As is well-known that the organic corrosion inhibitors have been studied and reported by different scholars mainly involving by molecular structure design, synthesis, characterization, corrosion inhibition evaluation and application. Usually the organic corrosion inhibitors, most of them contain heteroatoms, such as nitrogen atoms, sulfur atoms, oxygen atoms and so on [10-13]. These heteroatoms will cause inhibitor molecules to adsorb on metal surface, thus preventing the corrosion medium from attacking the metal to inhibitive corrosion.

Based on the structure-activity relationship of corrosion inhibitors, O,O'-diaryldithiophosphates and their derivatives can be used as a kind of effective inhibitors resulting the N, P and S atoms in the present in their structures. This has been confirmed by some of our previous works [14-16].

Here, as an extension study, but also for the development of new efficient corrosion inhibitor, S-benzyl-O,O'-bis(*p*-tert-butylphenyl)dithiophosphate (SOBP) as target inhibitor would be synthesized and characterized. Meanwhile, the inhibition performance of SOBP for Q235 steel in 1.0 M HCl would be studied by weight loss and potentiodynamic polarization measurement.

2. MATERIALS AND METHODS

2.1 Materials

All chemical reagents containing phosphorus pentasulphide (P_2S_5), *p*-tert-butylphenol (*p*-t-BuPhOH), diethylamine ($HNEt_2$), benzyl bromide (Bz-Br) and solvents involving toluene ($PhCH_3$), acetone (CH_3COCH_3), dichloromethane (CH_2Cl_2) are purchased from Chengdu Kelong Chemical Reagent Factory and Aladdin Chemistry Co., Ltd in this work, which all analytically pure chemicals. The 1.0 M HCl as the corrosion solution obtained by diluting concentrated hydrochloric acid with water (HCl, 37%). The test samples with the sizes of 2×25×50 mm (S = 28.0 cm^2) and the working electrode encapsulated by teflon with the working area of 0.785 cm^2 all prepared by Q235 steel.

2.2 Synthesis of SOBP

In order to synthesize the inhibitor of S-benzyl-O,O'-bis(*p*-tert-butylphenyl)dithiophosphate (SOBP, $(p\text{-t-BuPhO})_2PS_2CH_2Ph$), the precursor compound of O,O'-bis (*p*-tert- butyl phenyl) dithiophosphate diethyl ammonium ($(p\text{-t-BuPhO})_2PS_2NH_2Et_2$), was synthesized by the reaction of P_2S_5, *p*-t-BuPhOH and $HNEt_2$ in toluene based on previous works [14-16]. Then, SOBP was synthesized by $(p\text{-t-BuPhO})_2PS_2NH_2Et_2$ and Bz-Br in CH_2Cl_2 based on references [14-16]. The whole synthesis is carried out in two steps, the first step is the synthesis of precursor compound of (*p*-t-

$BuPhO)_2PS_2NH_2Et_2$, and the second step is the synthesis of target corrosion inhibitor of SOBP. The specific synthesis route is shown in figure 1. Finally, the synthesized corrosion inhibitor is colourless powder, yield 62.9%, melting range 86-87 °C.

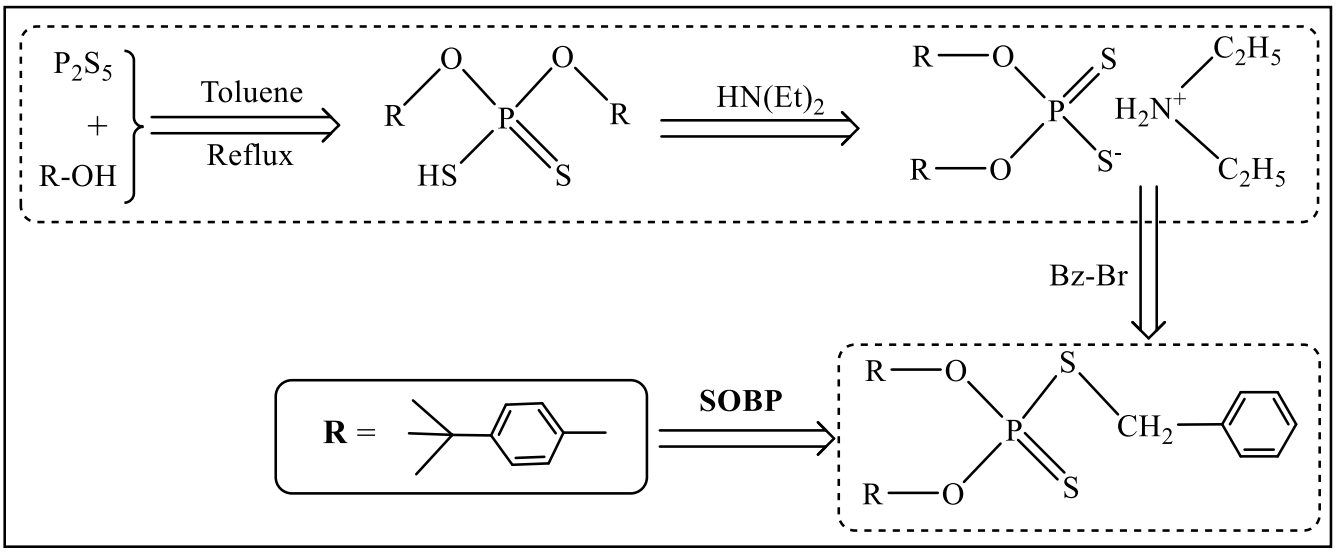

Figure 1. Synthetic route of SOBP.

2.3 Characterization of SOBP

In this work, in order to confirm the molecular structure of the corrosion inhibitor (SOBP), the elemental analysis (Carlo-Elba1106), fourier transform infrared spectrum (FT-IR, Nicolet-6700), nuclear magnetic resonance (^{1}H NMR, ^{13}C NMR and ^{31}P NMR, Brucker AV400) were chosen to characterize the composition and structural of synthesized corrosion inhibitor.

2.4 Performance evaluation

In weight loss measurements, the finely polished and dried Q235 steel samples were weighed on a digital balance with the accuracy of 1 mg. Then the samples were immersed in 1.0 M HCl solution in the absence and presence of the different SOBP at various temperatures for 8 h. After immersing, the tests samples were rinsed with distilled water, cleaned with acetone, dried and reweighed. The weight loss was calculated as the difference in weight of the sample before and after immersion in test solution of 1.0 M HCl[14, 17-18]. Here, the corrosion rate (v) and inhibition efficiency (IE_I, %) for Q235 steel corrosion in 1.0 M HCl with and without different concentrations of SOBP are calculated by equation (1) and (2). Where m_0 and m_i are the mass of the test specimen before and after corrosion, t is the immersion time, S = 28.0 cm^2, v_i and v_0 are corrosion rate of Q235 steel specimen in 1.0 M HCl with and without different concentrations SOBP.

$$v_i = \frac{m_0 - m_i}{St} \quad (1)$$

$$IE_{\mathrm{I}}\,(\%) = \frac{v_0 - v_i}{v_0} \times 100\% \qquad (2)$$

Potentiodynamic polarization measurement were conducted by conventional three-electrode system consisting of mild steel working electrode with an exposed area in 0.785 cm^2, a graphite electrode as counter electrode and saturated calomel electrode (SCE) as reference electrode employing by chi760e electrochemical workstation. All potential in this work were referred to the SCE. Before measurement, the working electrode was immersed in 1.0 M HCl as the test solution at open circuit potential (OCP) for 30 min to attain a stable state. The potential sweep rate for potentiodynamic polarization measurement was 0.5 mV s^{-1}. Corrosion current density (*I*) was determined from the intercept of extrapolated cathodic and anodic Tafel lines at the corrosion potential (*E*). The inhibition efficiency (IE_{II}, %) can be calculated by equation (3) [16, 19-20], where I_0 and I_{i} are the current densities of Q235 steel electrode in 1.0 M HCl without and with different concentrations SOBP.

$$IE_{\mathrm{II}}\,(\%) = \frac{I_0 - I_{\mathrm{i}}}{I_0} \times 100\% \qquad (3)$$

3. RESULTS AND DISCUSSION

3.1 Characterization of SOBP

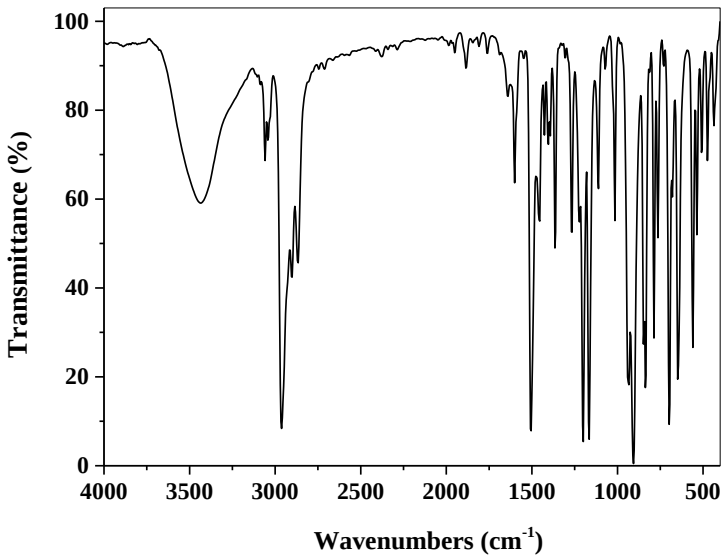

Figure 2. The FT-IR spectra of SOBP.

In order to confirm the inhibitor molecular structure of SOBP, the results of elemental analysis based on Anal. Calcd ($C_{27}H_{33}O_2PS_2$, Mr = 485): C, 66.80; H, 6.80; S, 13.20. Found: C, 66.92; H, 6.85; S, 13.24 showing that the chemical composition of the synthesized corrosion inhibitor is consistent with that of the target molecule.

In addition, based on the FT-IR (KBr, cm^{-1}) results showing figure 2, which presented that two absorption bands at 3041.9 (w) cm^{-1}, 3058.7 (w) contribute from the aromatic =*C*-*H* stretching, and three absorption bands at 1455.9 (w) cm^{-1},1505.9 (s) cm^{-1}, 1600.8 (w) cm^{-1} contribute from C=C stretching. The absorption bands of 2963.1 (s), 2901.9 (w) cm^{-1}, 2865.9 (s) cm^{-1} are attributed to the C-H (-CH_3, -CH_2-) stretching. Moreover, some absorption bands at 1110.3 (m) cm^{-1}, 1166.0 (s) cm^{-1}, 1200.7 (s) cm^{-1} and 906.9 (s) cm^{-1}, 934.8 (s) cm^{-1}, 1014.9 (m) cm^{-1} contribute from the (P)-O-C and P-O-(C) stretching, respectively[15, 21]. In addition, the absorption bands at 646.5 (s) cm^{-1}, 697.1 (s) cm^{-1}, 763.8 (s) cm^{-1}, 786.8 (m) cm^{-1}, 535.9 (m) cm^{-1}, 559.5 (s) cm^{-1} belong to the symmetric and asymmetric stretching vibrations of PS_2[15, 21].

^{1}H NMR δ/ppm: 1.35 (s, 18H, 2C(C*H*$_3$)$_3$), 4.27 (d, *J* = 15.41Hz, 2H, SC*H*$_2$), 7.16 -7.39 (m, 13H, Ph-*H*, 2C_6H_4Br). ^{13}C NMR, δ/ppm: 23.21 (*C*H_3), 31.92 (S*C*H_2), 38.92 (*C*(CH_3)$_3$), 120.21, 121.49, 125.79, 127.00, 127.06, 128.07, 128.50, 129.34, 148.52 (Ph-*C*, *C*$_6$H$_4$). ^{31}P NMR, δ/ppm: 89.03(t, *J* = 15.41 Hz).

Based on elemental analysis, FT-IR, ^{1}H NMR, ^{13}C NMR and ^{31}P NMR results, it can be found that the synthesized compound is the target corrosion inhibitor of SOBP seeing in figure 1.

3.2 Crystal structure of SOBP

A colorless block single crystal with dimensions 0.23 × 0.21 × 0.18 mm^3 was selected and used to determine the structure of SOBP by single crystal X-ray diffraction. All the crystal data were collected and summarized in table 1.

Table 1. Crystallographic data of SOBP.

Empirical formula	C_{27} H_{33} O_2 P S_2
Formula weight	484.62
Crystal system	Triclinic
Space system	*P*-1
Temperature [K]	296 (2)
a [Å]	9.118 (6)
b [Å]	10.227 (6)
c [Å]	15.848 (9)
A [°]	79.091 (10)
B [°]	86.968 (11)
γ [°]	68.185 (9)
V [Å^3]	1346.9 (14)
Z	2
R_{int}	0.0202
F (000)	516
D_c [kg·m^{-3}]	1.195
μ (Mo $K\alpha$) [mm^{-1}]	0.71073
Crystal size [mm^3]	0.23 × 0.21 × 0.18
Goodness-of-fit on S^2	1.027
R indices (all data)	R_1 = 0.0885, wR_2 = 0.1385

Limiting indices	$-10 \le h \le 11$, $-13 \le k \le 13$, $-12 \le l \le 21$
θ range for data collection [°]	2.18 ~ 28.81 °
Data/restraints/parameters	6410 / 6 / 358
Final R indices [$I > 2\sigma(I)$]	$R_1 = 0.0469$, $wR_2 = 0.1173$
Largest diff. peak and hole [e.nm^{-3}]	0.200, - 0.247
$w = 1/[\sigma^2(F_o^2) + (a\ P)^2 + bP]$	$a = 0.0637$, $b = 0.000$, $P = (F_o^2+2F_c^2)/3$

The ORTEP view of the single-crystal X-ray structure of SOBP is presented in figure 3, and the selected bond distances and angles are also listed in table 2 and 3. According to table 1, which shows that the compound of SOBP is crystallized in the Triclinic group *P*-1. A distorted tetrahedral environment around P atom (P1) can be clearly seen with two O atoms (O1 and O2) and two S atoms (S1 and S2) bonded to the central P atom showing in figure 3. The bond lengths of P1-S1 and P1-S2 in SOBP are 1.9204 (12) Å and 2.0539 (14) Å respectively, which are close to the corresponding bond length (P1–S2and P1-S2) presenting in covalent compound of S-benzyl-O,O'-bis(2-naphthyl) dithiophosphate (1.896 (3) and 2.051 (3) Å) [15], and it also distinct from the ionic compound of *N*, *N*-diethyl ammonium *O*, *O*'-di(methyl phenyl)dithiophosphate (0.1971 (15) Å and 0.1942(15) Å) [22]. The significant differences in the bond lengths of P1-S1 and P1-S2 in covalent compound indicate the existence of single bond (P-S) and double bond (P=S) in covalent compounds, while the two bond (P1-S1 and P1-S2) lengths in ionic compounds are relatively close, indicating that there is no obvious P-S bond and P=S bond, which is mainly due to the obvious conjugation of P-S bond and P=S bond.

Table 2. Selected bond distances (Å) of SOBP.

Bonds	Distances (Å)	Bonds	Distances (Å)	Bonds	Distances (Å)
S1-P1	1.9204 (12)	C8-C13	1.357 (3)	C18-C19	1.372 (3)
S2-C1	3.645 (2)	C8-C9	1.361 (3)	C18-C23	1.374 (3)
S2-P1	2.0539 (14)	C9-C10	1.388 (3)	C19-C20	1.389 (3)
P1-O1	1.6031 (16)	C10-C11	1.381 (3)	C20-C21	1.386 (3)
P1-O2	1.6037 (17)	C11-C12	1.385 (3)	C21-C22	1.390 (3)
O1-C18	1.415 (2)	C11-C14	1.539 (3)	C21-C24	1.540 (3)
O2-C8	1.418 (3)	C12-C13	1.392 (3)	C22-C23	1.389 (3)
C1-C2	1.500 (3)	C14-C16B	1.465 (10)	C24-C27B	1.503 (7)
C2-C3	1.379 (3)	C14-C15	1.490 (7)	C24-C27	1.513 (8)
C2-C7	1.385 (3)	C14-C17	1.539 (7)	C24-C25	1.525 (8)
C3-C4	1.384 (3)	C14-C16	1.557 (6)	C24-C26B	1.546 (6)
C4-C5	1.353 (4)	C14-C15B	1.586 (9)	C24-C26	1.548 (8)
C5-C6	1.365 (4)	C14-C17B	1.601 (9)	C24-C25B	1.564 (6)
C6-C7	1.400 (4)				

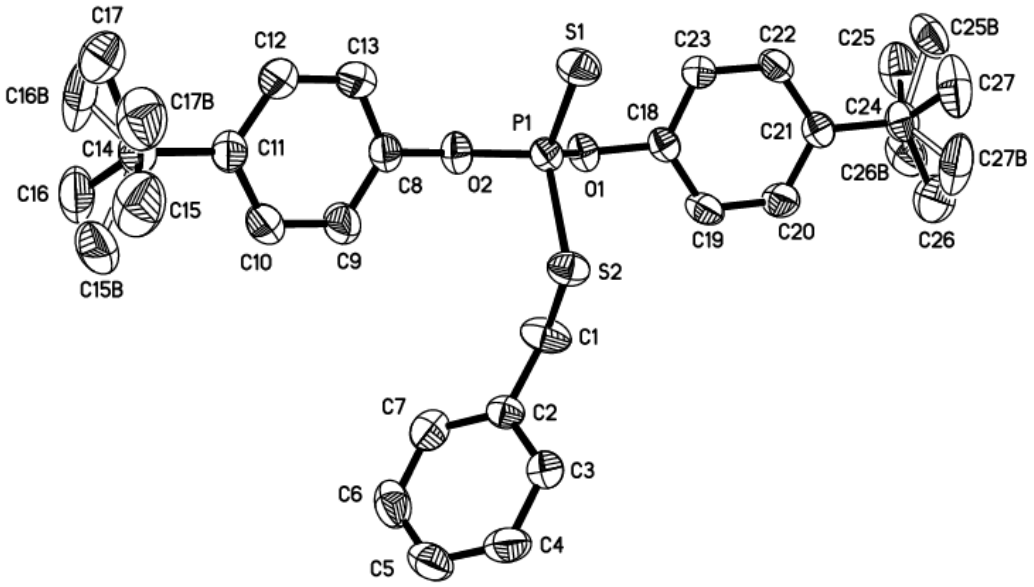

Figure 3. ORTEP view of SOBP with displacement ellipsoids at the 30% probability level.

Table 3. Selected bond angles of SOBP.

Bonds	Angles (°)	Bonds	Angles (°)	Bonds	Angles (°)
C1-S2-P1	103.46 (10)	C8-C9-C10	119.8 (2)	C23-C18-O1	120.46 (19)
O1-P1-O2	92.66 (9)	C11-C10-C9	122.4 (2)	C18-C19-C20	119.2 (2)
O1-P1-S1	118.04 (7)	C10-C11-C12	115.6 (2)	C21-C20-C19	122.5 (2)
O2-P1-S1	117.59 (7)	C10-C11-C14	121.2 (2)	C20-C21-C22	116.4 (2)
O1-P1-S2	109.12 (7)	C12-C11-C14	123.2 (2)	C20-C21-C24	122.4 (2)
O2-P1-S2	108.67 (7)	C11-C12-C13	122.7 (2)	C22-C21-C24	121.2 (2)
S1-P1-S2	109.52 (5)	C8-C13-C12	119.3 (2)	C23-C22-C21	122.0 (2)
C18-O1-P1	122.53 (14)	C15-C14-C17	111.2 (5)	C18-C23-C22	119.5 (2)
C8-O2-P1	122.44 (14)	C16B-C14-C11	110.1 (4)	C27-C24-C25	110.8 (6)
C2-C1-S2	110.63 (16)	C15-C14-C11	109.0 (3)	C27B-C24-C21	108.3 (3)
C3-C2-C7	118.2 (2)	C17-C14-C11	111.2 (4)	C27-C24-C21	109.4 (3)
C3-C2-C1	120.6 (2)	C15-C14-C16	110.9 (5)	C25-C24-C21	107.3 (4)
C7-C2-C1	121.2 (2)	C17-C14-C16	106.3 (5)	C27B-C24-C26B	111.3 (5)
C2-C3-C4	120.9 (2)	C11-C14-C16	108.2 (3)	C21-C24-C26B	109.2 (3)
C5-C4-C3	120.8 (3)	C16B-C14-C15B	111.1 (7)	C27-C24-C26	109.4 (7)
C4-C5-C6	119.6 (3)	C11-C14-C15B	113.5 (4)	C25-C24-C26	108.4 (6)
C5-C6-C7	120.5 (3)	C16B-C14-C17B	109.7 (7)	C21-C24-C26	111.4 (4)
C2-C7-C6	120.0 (3)	C11-C14-C17B	109.1 (4)	C27B-C24-C25B	109.9 (5)
C13-C8-C9	120.2 (2)	C15B-C14-C17B	103.1 (6)	C21-C24-C25B	113.1 (3)
C13-C8-O2	120.2 (2)	C19-C18-C23	120.3 (2)	C26B-C24-C25B	105.0 (4)
C9-C8-O2	119.4 (2)	C19-C18-O1	119.06 (19)		

In addition, the tertiary butyl on the benzene ring is in a disordered state, in which the shares of C15, C16 and C17, C15B, C16B and C17B, C25, C26 and C27, C25B, C26B and C27B are 0.586 (10), 0.414 (10), 0.448 (9) and 0.552 (9). Here, the tertiary butyl disorder due to the rotation of the sigma bond.

3.3 Weight loss measurement

The effect of SOBP concentration (c, mg L^{-1}) on inhibition efficiency (IE_I, %) for Q235 steel in 1.0 M HCl at 303 K by weight loss measurement is presented in figure 4. It can be found that the inhibition efficiency increases with the increase of the concentration of SOBP. Inhibition efficiency significantly increases with the concentration of SOBP increases from 0 mg L^{-1} to 100 mg L^{-1}, when the concentration of SOBP exceeds 100 mg L^{-1}, the inhibition efficiency increases slightly, which tends to be stable as the concentration of inhibitor SOBP. The slightly change of inhibition efficiency is due to the saturation adsorption of SOBP on Q235 steel surface. With the concentration of corrosion inhibitor increases to 100 mg L^{-1} and 200 mg L^{-1}, the inhibition efficiency are 93.87% and 94.21%, respectively. The higher inhibition efficiency indicates that the inhibitor of SOBP is an effective corrosion inhibitor.

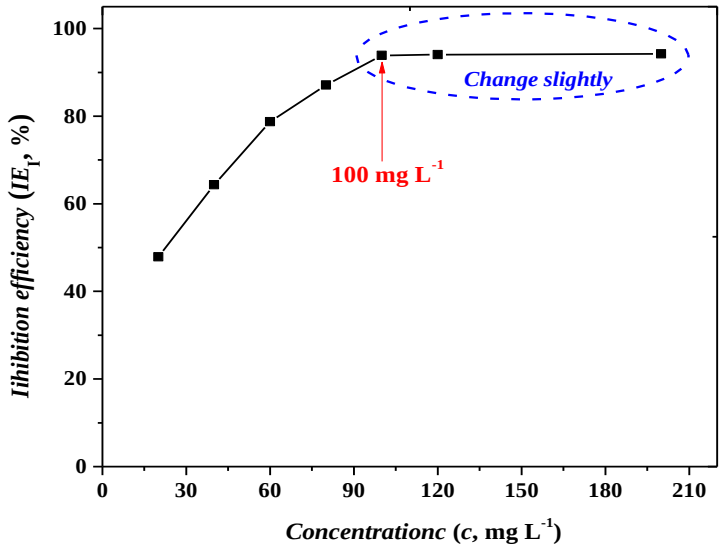

Figure 4. The effect of SOBP concentration on inhibition efficiency (IE_I, %) for Q235 steel in 1.0 M HCl at 303 K.

3.4 potentiodynamic polarization measurement

Potentiodynamic polarization curves obtained by potentiodynamic polarization measurement for Q235 steel corrosion in 1.0 M HCl with different concentrations of SOBP at 303 K is shown in figure 5. Here, the inhibition efficiency (IE_{II}, %), corrosion current density (I_i, μA cm^{-2}), corrosion potential (E vs SCE, V), cathodic and anodic Tafel slopes (β_c and β_a, mV dec^{-1}) are listed in table 5.

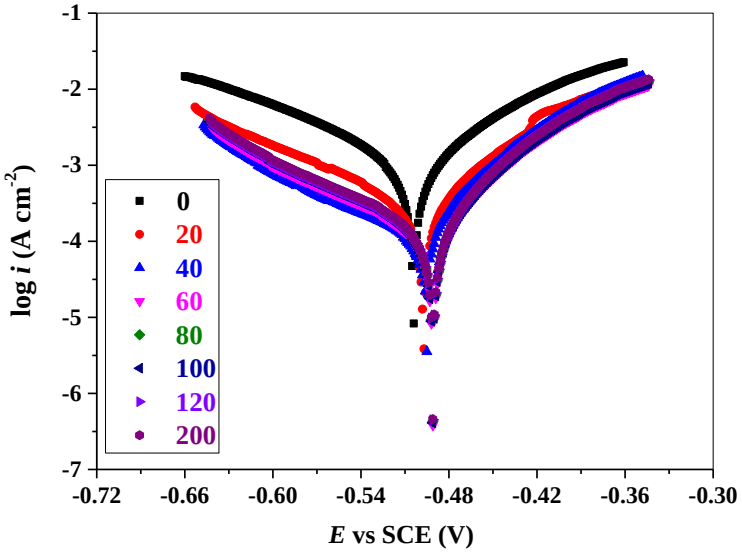

Figure 5. Potentiodynamic polarization curves for Q235 steel in 1.0 M HCl with various concentrations of SOBP at 303 K.

Table 5. Electrochemical parameters for Q235 steel in 1.0 M HCl with various concentrations of SOBP at 303 K.

c (mg L^{-1})	E (mV)	β_a (mV dec^{-1})	β_c (mV dec^{-1})	I_i (μA cm^{-2})	IE_{II} (%)
0	-496	131	113.3	1938.4	-
20	-496	125	101.5	1232.1	36.4
40	-495	111	100.6	820.5	57.7
60	-488	108	97.9	478.6	75.3
80	-486	105	96. 4	340.2	82.5
100	-486	104	95.2	187.4	90.3
120	-485	100	94.4	119.0	93.9
200	-480	97	87.0	116.9	94.4

From figure 5 and table 5, both anodic and cathodic curves shift to lower current densities for Q235 steel in 1.0 M HCl with SOBP concentration increased. The decrease of corrosion current density is due to the corrosion inhibitor adsorbing on Q235 steel surface to form a protective film, thus preventing the attack of hydrogen ions on iron atoms. In addition, cathodic and anodic Tafel slopes all decrease as the concentration of inhibitor increases, while inhibition efficiency increases as the concentration of inhibitor increases. As the SOBP concentration increased from 20 mg L^{-1} to 120 mg L^{-1}, the inhibition efficiency increased from 36.44% to 93.86%, with the further increase of SOBP concentration, the inhibition efficiency increased slightly. This is due to the corrosion inhibitor of SOBP adsorption on Q235 steel surface has reached saturation. Additionally, all corrosion potential for Q235 steel in 1.0 M HCl with various concentration of SOBP at 303 K shifts less than 20 mV ($<$85 mV), which shows that SOBP is a mixed-type inhibitor [6, 8].

3.5 Adsorption isotherm

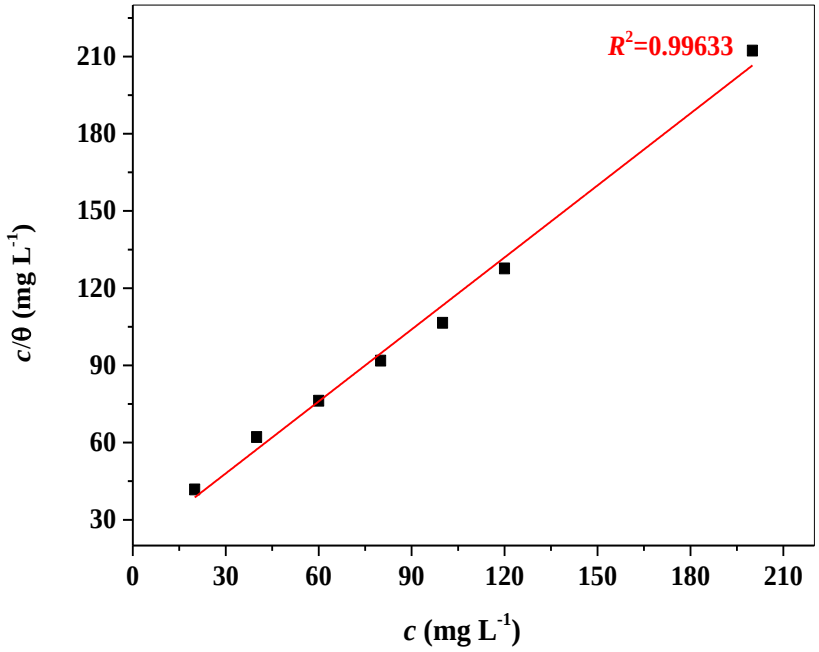

Figure 6. The plots of Langmuir adsorption isotherm for SOBP on Q235 steel in 1.0 M HCl at 303 K.

In this work, only the data of weight loss measurement are selected for adsorption isotherm analysis. According to the data of weight loss measurement showing in figure 4, various isotherms containing Langmuir adsorption isotherms (seeing equation (4) and (5).) are used to present the adsorption of SOBP on Q235 steel surface in 1.0 M HCl solution. Meanwhile, the strong correlation (R^2=0.99633, see figure 6) of fitting result presenting in figure 6 suggest that the adsorption of SOBP on Q235 steel surface obey Langmuir adsorption isotherm. In addition, the adsorption free energy (ΔG, kJ mol^{-1}) for SOBP on Q235 steel in 1.0 M HCl solution at 303 K can be calculated by the fitting results according to equation (6), the calculated ΔG is -35.55 kJ mol^{-1} and higher than -40.00 kJ mol^{-1}, which also indicates that the adsorption of SOBP on Q235 steel surface in 1.0 M HCl belongs both physisorption and chemisorption [16, 23]. Where c is SOBP concentration, K_A is the adsorption equilibrium constant and θ is the surface coverage, v_i and v_0 are the corrosion rate of Q235 steel corrosion in 1.0 M HCl with and without different concentrations of inhibitor.

$$\frac{c}{\theta} = \frac{1}{K_A} + c \quad (4)$$

$$\theta = \frac{v_0 - v_i}{v_0} \quad (5)$$

$$\Delta G = -RT\ln(55.5K) \quad (6)$$

4. CONCLUSIONS

In conclusion, the target compound of S-benzyl-O,O'-bis(*p*-tert-butyl phenyl)dithiophosphate (SOBP) as new corrosion inhibitor was synthesized and characterized. Study results indicate that

SOBP is an effective mixed-type corrosion inhibitor, and the corrosion inhibition increases with the concentration of SOBP. The adsorption of SOBP on Q235 steel surface in 1.0 M HCl obey Langmuir adsorption isotherm, which belongs to both physisorption and chemisorption.

ACKNOWLEDGMENTS
This project is supported financially by the program of Science and Technology Department of Sichuan Province (Nos. 2018JY0061, 2017JY0180), the program of Education Department of Sichuan Province (No. 18CZ0038), the opening project of Material Corrosion and Protection Key Laboratory of Sichuan Province (No. 2017CL02), the opening project of Key Laboratories of Fine Chemicals and Surfactants in Sichuan Provincial Universities (Nos. 2018JXZ01, 2016JXZ03), the opening project of Key Laboratories of Green Catalysis of Higher Education Institutes of Sichuan (No. LZJ1803) and the projects of Sichuan University of Arts and Science (Nos. 2018SCL001Z, 2018KC005Z).

References

1. J. Šćepanović, D. Radonjić and D. Vuksanović, *Int. J. Electrochem. Sci*., 13 (2018) 8623.
2. P. A. Lozada, O. O. Xometl, N. V. Likhanova, I. V .Lijanova, J. R.Vargas-García and R. E. H. Ramírez, *J. Mol. Liq.,* 265 (2018) 151.
3. A. A. Al-Amierya, M. H. O. Ahmed, T. A. Abdullahc, T. S. Gaazd and A. A. H. Kadhum, *Results Phys.,* 9 (2018) 978.
4. H. J. Habeeb, H. M. Luaibi, R. M. Dakhil, A. A. H. Kadhum, A. A. Al-Amiery and T. S. Gaaz, *Results Phys*., 8 (2018) 1260.
5. E. Naseri, M. Hajisafari, A. Kosari, M. Talari, S. Hosseinpour and A. Davoodi, *J. Mol. Liq*., 269 (2018) 193.
6. S. Varvara, L. Găină, R. Bostan, F. Popa and A.Grozav, *Int. J. Electrochem. Sci*., 13 (2018) 8338.
7. A. Mahsoune, K. Sadik, M. E. Belghiti, I. Bahadur and A. Aboulmouhajir, *Int. J. Electrochem. Sci*., 13 (2018) 8396.
8. D. Fu, B. Tan, L. Lu, X.Qin, S. Chen, W.He and J. Chen, *Int. J. Electrochem. Sci*., 13 (2018) 8561.
9. M. Mobin, M. Basik and J. Aslam, *J. Mol. Liq*., 263 (2018)174.
10. M. Goyal, S. Kumar, I. Bahadur, C. Verma and E. E. Ebenso, *J. Mol. Liq*., 256 (2018) 565.
11. S. A. Umoren, A. A. AlAhmary, Z. M. Gasem and M. M. Solomon, *Int. J. Biol. Macromol*., 117 (2018)1017.
12. A. E. Somers, B. R. W. Hinton, C. B. Dickason, G. B. Deacon, P. C. Junk and M. Forsyth, *Corro. Sci.*, 139 (2018) 430.
13. J. Zhang, L. Zhang, G. Tao and N. Chen, *Int. J. Electrochem. Sci*., 13 (2018) 8645.
14. C. Lai, X. Guo, J. Wei, B. Xie, L. Zou, X. Li, Z. Chen and C. Wang, *Open Chem*., 15 (2017) 263.
15. C. D. Wang, C. Lai, B. Xie, X. G. Guo, D. Fu, B. Li and S. S. Zhu, *Results Phys.,* 10 (2018) 558.
16. C. Lai , B. Xie, L. Zou , X. Zheng , X. Ma and S. Zhu, *Results Phys*., 7 (2017) 3434.
17. M. H. O. Ahmed, A. A. Al-Amiery, Y. K. Al-Majedy, A. A. H. Kadhuma, A. B. Mohamad and T. S. Gaaz*, Results Phys.,* 8 (2018) 728.
18. X. Wang, S. Ren, D. Zhang, H. Jiang and Y. Gu, *Int. J. Electrochem. Sci.,* 13 (2018) 9888.
19. H. Yang, M. Zhang and A. Singh, *Int. J. Electrochem. Sci*., 13 (2018) 9131.
20. A. Kadhima, A. K. Al-Okbi, D. M. Jamil, A. Qussay, A. A. Al-Amiery, T. S. Gaaz, A. A. H. Kadhum, A. B. Mohamad and M. H. Nassir, *Results Phys*., 7 (2017) 4013.
21. K. Wang, C. Lai, B. Tan, B. Xie, S. Zhu, H. Zhu, K. Liu and J. Wei, *Int. J. Electrochem. Sci*., 13 (2018) 2627.
22. B. Xie, C. Lai, Y. Xiang, L. Zou, Z. Xiang, C. Huang and B. Yi, Chinese *J. Appl. Chem.,* 29 (2012) 200.

23. M. A. El-Raouf, E. A. Khamis, M. T. H. A. Kana and N. A. Negm, *J. Mol. Liq.,* 255 (2018) 341.